Cross-sectional scanning tunneling microscope study of a boron-implanted Si wafer

H. Hirayama
Department of Material Science and Engineering, Tokyo Institute of Technology, 4259 Nagatsuda, Midori-ku, Yokohama, 226, Japan

M. Koike*
Department of Physics, Tokyo Institute of Technology 2-12-1 Ohokayama, Meguro-ku, Tokyo 152, Japan

Y. Einaga
Department of Material Science and Engineering, Tokyo Institute of Technology, 4259 Nagatsuda, Midori-ku, Yokohama 226, Japan

A. Shibata†
Department of Physics, Tokyo Institute of Technology 2-12-1 Ohokayama, Meguro-ku, Tokyo 152, Japan

K. Takayanagi
Department of Material Science and Engineering, Tokyo Institute of Technology, 4259 Nagatsuda, Midori-ku, Yokohama 226, Japan
(Received 9 August 1996; revised manuscript received 3 March 1997)

We cleaved a boron (B) heavily implanted Si wafer, and observed its (111) cross section using a scanning tunneling microscope (STM). After annealing, the characteristic $(\sqrt{3}\times\sqrt{3})R30°$ reconstruction of the B-rich Si(111) surface appeared at the edge where the implanted B accumulated. The 7×7 reconstruction was observed in the middle of the cleaved surface where the implanted B was absent. Between the 7×7 and the $\sqrt{3}\times\sqrt{3}$ reconstructions, a transient region with a disordered phase was observed. The disordered phase nucleated just under the step edge, and connected to the 7×7 domain in the middle of the lower terrace. The boundary between the disordered phase and the 7×7 domain was straight along the $[\bar{1}10]$ direction and was terminated by faulted halves of the dimer-adatom-stacking fault (DAS) 7×7 unit cell. At the boundary, adatoms in the disordered phase are arranged to construct the corner hole of the DAS structure. However, they do not introduce a stacking fault into the disordered phase. In the disordered phase, $\sqrt{3}\times\sqrt{3}$ domains existed locally, and were separated by out-of-phase boundaries with $c(2\times4)$ and/or 2×2 local atomic arrangements in relation to each other. By the sample bias voltage dependence of the STM image, we found that all the $c(2\times4)$ and the 2×2 local atomic arrangements are due to the Si adatom at $T4$ site on the subsurface Si atom, whereas the $\sqrt{3}\times\sqrt{3}$ domains are due to the B atom at $S5$ subsurface site under the Si adatom. At the transient region where the B coverage is less than the saturation value to complete the B-induced $\sqrt{3}\times\sqrt{3}$ reconstruction, the condensation of the B atom into $\sqrt{3}\times\sqrt{3}$ local domains results in the B-deficient region with the $c(2\times4)$ and 2×2 local adatom arrangement between $\sqrt{3}\times\sqrt{3}$ local domains. With respect to the local surface energy, the B-rich and the B-deficient surface favors the $\sqrt{3}\times\sqrt{3}$ and the 2×2 and/or $c(2\times4)$ adatom arrangement, respectively. The coexistence of these local domains causes the disordered phase. [S0163-1829(97)03627-8]

I. INTRODUCTION

Among column III atoms of a p-type dopant in silicon, boron (B) is the most popular impurity. It is because of its high solubility and small diffusion coefficient in crystalline Si. These characteristics of the B dopant are suitable to fabricate a thin p-type layer of a high dopant concentration, which is one of the key points in the down-sizing of microelectronics devices.[1] Usually, the thin p-type layer is realized by low-energy (~30 KeV) ion implantation of B into the crystalline Si wafer.[2] The implanted B does not reach to the depth of ~1 μm, so that the implanted B accumulated in the shallow layer of the wafer surface. The concentration of the implanted B atom drastically changes from an extremely high to a negligible value at ~1 μm depth. The atomic structure of this transient region is of interest both from the scientific and technological points of view. In this study, we cleaved a B-implanted Si(111) wafer and investigated the atomic arrangement of the transient region on its $(\overline{111})$ cleavage surface with a scanning tunneling microscope (STM).

The clean Si(111) surface is well known to show the dimer-adatom-stacking fault (DAS) 7×7 reconstruction.[3] However, the B-rich Si(111) surface has been reported to show the $(\sqrt{3}\times\sqrt{3})$ $R30°$ reconstruction[4] with the saturation coverage of $\sim\frac{1}{3}$ ML.[5] This $\sqrt{3}\times\sqrt{3}$ reconstruction has been found to originate from the B atom at the subsurface $S5$ site under the Si adatom at the $T4$ site using a combination of scanning tunneling spectroscopy (STS) and the theoretical calculation.[6–8] For the B coverage of less than $\frac{1}{3}$ ML, the atomic arrangement of the Si(111) surface has been also reported in recent studies.[9–11] Shen *et al.*[9] controlled the surface B concentration by a combination of quenching and the subsequent annealing of the highly B-doped $(2\times10^{19}$ cm$^{-3})$ Si(111) wafer. The quenching resulted in a disordered 1×1 phase with local 2×2 and $c(2\times4)$ ar-

 © 1997 The American Physical Society

rangements inside the 7×7 reconstruction as is usually observed in the quenching of the Si(111) surface with a low concentration of both a p- and n-type dopant.[12–15] However, a part of the 1×1 region changed to the B-induced $\sqrt{3}\times\sqrt{3}$ domain in the subsequent annealing, though the disordered 1×1 phase still remained between the 7×7 and the $\sqrt{3}\times\sqrt{3}$ domains. The surrounding 7×7 reconstruction was terminated by the faulted half of the DAS unit cell. Wong, Mckinnon, and Welland[10] also studied the quenched and annealed surface of the highly B-doped ($\sim10^{19}$ cm^{-3}) Si(111) wafer. On the surface, the 7×7 and the defective $\sqrt{3}\times\sqrt{3}$ domain coexisted. The 7×7 reconstructions was reported to be terminated by the unfaulted half of the DAS unit cell. They proposed an abrupt boundary between the 7×7 and the $\sqrt{3}\times\sqrt{3}$ domains with an extra dimer row on the base of their STM observation. Zotov *et al.* studied the the Si(111) surface of small B coverages and observed 2×2, $c(2\times4)$ local atomic arrangements, ringlike clusters, and deep holes as defects in the $\sqrt{3}\times\sqrt{3}$ reconstruction.[11]

These previous studies suggest that the 7×7 and the $\sqrt{3}\times\sqrt{3}$ domain coexist on the Si(111) surface with a small B coverage. The 7×7 reconstruction is terminated by halves of the DAS unit cell at the boundary to the $\sqrt{3}\times\sqrt{3}$ domain. The $\sqrt{3}\times\sqrt{3}$ is defective. However, we find inconsistency on the kind of terminating halves of the 7×7 DAS unit cell and the existence of the intermediate 1×1 phase between the 7×7 and the $\sqrt{3}\times\sqrt{3}$ domain. We think that the confusion comes from the quenching process which was adapted to control the surface B concentration in the previous studies. In previous studies, the used Si(111) wafer had a B dopant concentration of $\sim10^{19}$ cm^{-3}. In this range of the dopant concentration, heating at a high temperature was necessary to segregate B atoms to the surface. But, the segregated B atom would return during the subsequent cooling process as to attain the thermally equilibrium distribution of B atoms if the sample could be cooled down slowly. To prevent the segregated B atom from returning to the bulk, the rapid cooling (i.e., the quenching) process was adapted. But, the quenched Si(111) surface has an intrinsic nature to show such metastable structures as 2×2, $c(2\times4)$, $\sqrt{3}\times\sqrt{3}$ reconstruction inside the 7×7 reconstruction.[12–15] Thus, we should consider both the B concentration and the metastable nature of the intrinsic Si(111) surface as causes of the surface structure observed in previous studies. These indistinguishable causes gave a variety of the observed surface structure.

In this study, we prepared a heavily B-implanted Si(111) wafer and observed its {111} cleaved cross section by STM. The implanted B atom was accumulated in a narrow region just under the wafer surface. The B concentration of the accumulated region is supposed to be $\sim10^{21}$ cm^{-3}, which is two orders of magnitude larger than the sample used in the previous studies. Due to the large B concentration, the $\sqrt{3}\times\sqrt{3}$ structure appeared at the B accumulated region without the quenching process. Moreover, the B concentration distributed spatially on the cleaved cross section from an extremely large to a negligible value. Hence, without considering the quench-induced metastable structure, we could directly study the effect of the B concentration on the Si(111) surface structure by observing the spatial change of the STM image. On the base of previous studies, we anticipate that the local structure will change from the $\sqrt{3}\times\sqrt{3}$ to the 7×7 reconstruction in the travel from the B-accumulated region toward the B-unimplanted region on the cleaved cross-sectional surface. But, still we do not know how the local structure changes at the transient region where the B concentration drastically changes from an extremely high to a negligible value. Do we observe a continuously changing intermediate local structure as expected from the drastic, but continuous spatial change of the implanted B concentration? Or, does some critical B concentration exist for the phase separation into the $\sqrt{3}\times\sqrt{3}$ and the 7×7 domain? In the following, we examine how the distribution of the implanted B atom acts on the surface local structure at the cleaved cross-sectional surface.

II. EXPERIMENT

The B-doped ($\sim10^{17}$ cm^{-3}) Si(111) wafer was used as a substrate. Into this wafer, extra B atoms were introduced by 30-KeV BF_2^+ ion implantation. The dosage of BF_2^+ ion was as large as 1×10^{17} cm^{-2}. In the 30-KeV implantation of BF_2^+ ion, the implanted B is accumulated in a shallow region of ~1 μm of the wafer's surface.[16] We confirmed the depth profile of implanted B using a chemical etching sensitive to the B concentration.[17] At ~1 μm stained layer of a high B concentration was observed at the edge of the cleaved cross section of the implanted wafer by a scanning electron microscope. The implantation of B atoms causes the B concentration of $\sim10^{21}$ cm^{-3} in the accumulated region.

For STM observation, the B-implanted (111) wafer was cut into 5×7 mm pieces. A guide line was scratched along $[\bar{1}10]$ direction on the backside of the sample to expose $(\bar{1}\bar{1}1)$ surface by cleavage. Then the sample was degreased and was mounted on a STM sample holder specially designed for the cleavage. The sample was mounted obliquely so that the $(\bar{1}\bar{1}1)$ cleavage surface is normal to the STM tip. The sample was cleaved by pushing the upper part of the sample with a blade which glided parallel to $(\bar{1}\bar{1}1)$ cleavage surface. This exposed the $(\bar{1}\bar{1}1)$ cleaved surface which was the subject of our STM observation.

The STM used is a modification of a commercially available system (JEOL JSTM-4500XV). Tips of STM were made by electrochemical etching of 0.30-mm-diameter *W* wires. The STM images were obtained at a constant current of 0.3 nA. The sample bias was changed in the range from -2.0 to $+2.0$ V. Images are shown with a conventional gray scale keyed to the surface height. The cleavage exposed the $(\bar{1}\bar{1}1)$ cleaved surface of the ~300 μm width, on which the tip was approached. However, the transient region of interest was located in the narrow region of ~1 μm at the mirror-polished surface side edge on the cleaved surface. Thus, we sequentially searched the transient region by moving the observation point at intervals of 0.5 μm from the approaching point toward the mirror-polished side edge on the cleaved cross-sectional surface. At the region close to the edge, the topograph was sampled at intervals of 0.1 μm.

The STM observation was performed in our UHV apparatus which consisted of three chambers; the loading chamber, the sample preparation chamber with the cleavage mechanism, and the main chamber with a STM unit. The base pressure of the preparation and the main chambers were

less than 1×10^{-8} and 8×10^{-9} Pa, respectively. To observed the as-cleaved surface, we cleaved the sample in the preparation chamber. Before the cleavage, the sample was outgased at 500 °C for several hours in the preparation chamber. Then, the sample was cooled down to the room temperature and was cleaved. We observed the cleaved cross-sectional surface using a STM just after the cleavage. However, for the cleaved surface after the annealing process described in the next section, we found no difference in the STM image between the samples cleaved in vacuum and in air. Thus, STM images of the cleaved surface after the annealing were taken on both the sample cleaved in vacuum and the air. For both the as-cleaved surface and the surface after the annealing, the STM observation was performed at room temperature.

III. RESULTS

Just after the cleavage, the atomically resolved 2×1 reconstruction was clearly observed in the middle of the cleaved surface by a STM. The STM images of the 2×1 structure was confirmed to show the same bias dependence as the π-bonded chain structure,[18–22] which appears on the cleaved Si(111) surface. Thus, it is reasonable that the 2×1 reconstruction was widely observed in the middle part of our cleaved surface where the implanted B atom did not reach. However, as the tip samples the area more close to the near-edge region, the step density was noticed to increase. At the very edge region where the implanted B atom was accumulated, no atomically resolved image could be obtained because the surface was too rough to follow the surface height in our STM feedback system. The roughness might have resulted from the defects in the Si matrix at the edge region which could be introduced by the large dosage of the implantation.[23]

The annealing after the cleavage made the near-edge region flatter and enabled us to observe atomically resolved STM images at several points on the B accumulated region. The annealing process of this study was as follows. First, the sample was flashed at 1200 °C for 90 sec, and was kept at 1000 °C for 20 min. Then, the sample was slowly cooled down to room temperature with the cooling rate of less than 1 °C/sec. Because of this slow, quasistatic cooling process, the sample surface fell into the most stable state. In fact, we examined the surface of the Si(111) wafer of a small concentration of n-type dopant in the same annealing process and confirmed that no such metastable structures as $c(2\times4)$, 2×2, and $\sqrt{3}\times\sqrt{3}$ local reconstruction appeared on the surface, but the 7×7 structure appeared entirely. The annealing should enhance the boron diffusion. This would modify the original distribution of the implanted B atom in the sample. However, no drastic change was observed in the local structure of the cleaved surface in repeating the annealing process. Thus, we think that the diffusion has no significant effect on the local structure of the cleaved surface. The local structure of the cleaved surface is determined by the local concentration of the B atom.

After the heat treatment of the B-implanted Si specimen, the 7×7 reconstruction was observed on wide terraces in the middle of the cleaved $(\bar{1}\bar{1}1)$ surface. The 2×1 reconstruction is metastable and is easy to change irreversibly to the

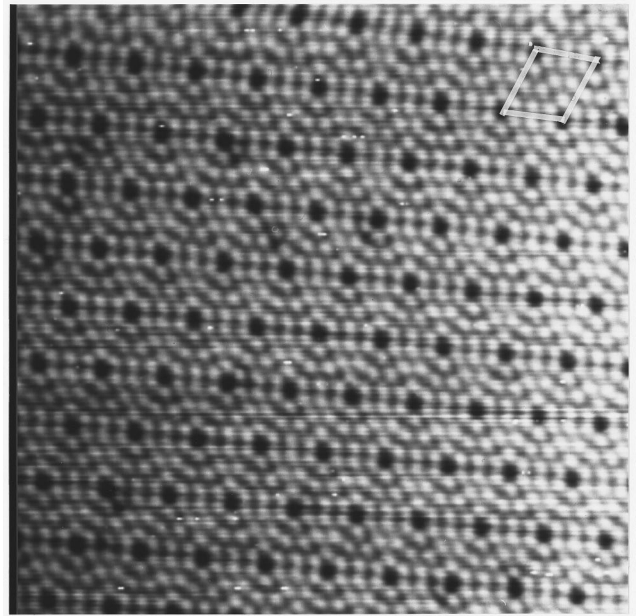

FIG. 1. A 30×30 nm^2 empty state image of the 7×7 reconstruction which appeared in the middle of the cleaved surface after the heat treatment. The sample bias voltage was $+2.0$ V. The tunneling current was 0.3 nA. A unit cell of the 7×7 reconstruction is indicated at the upper right corner of the figure.

energetically stable 7×7 DAS reconstruction of the Si{111} surface after the heating above $\sim$400 °C.[22] Therefore, the 7×7 reconstruction was widely observed in the middle of the cleaved {111} surface on the unimplanted region. A typical STM image is shown in Fig. 1. The adatom site[24,25] was observed as the bright protrusion in the positive sample bias STM. The brightness of the protrusion was noticed to be even.

Traveling from the middle to the edge region on the cleaved surface, we crossed an immense area of the 7×7 reconstruction with steps between large terraces. Then, we crossed a transient region. At the final stage of the travel, we encountered the perfect $\sqrt{3}\times\sqrt{3}$ reconstruction. Figure 2 shows an example of the observed STM image of the $\sqrt{3}\times\sqrt{3}$ reconstruction. Since a large amount of B atom causes the B-induced $\sqrt{3}\times\sqrt{3}$ reconstruction,[5–7] it is reasonable that the $\sqrt{3}\times\sqrt{3}$ reconstruction appeared on the edge region where the implanted B atom was accumulated.

In the transient region between the 7×7 and the $\sqrt{3}\times\sqrt{3}$ reconstruction, we found the disordered phase shown in Fig. 3. Here, the lower ride of the image is closer to the region of the 7×7 reconstruction (i.e., B-unimplanted area). In the lower part of the figure, a double-layer height step was observed. The step edge was straight and was found to terminate by unfaulted halves of the 7×7 DAS unit cell. Just under the step edge, the disordered structure was nucleated. The disordered phase was connected to the 7×7 reconstruction on the terrace in the upper area of the image. The 7×7 area then changed to the $\sqrt{3}\times\sqrt{3}$ at regions further away from the upper area. We found that the boundary between the disordered phase and the 7×7 reconstruction was terminated by faulted halves of the DAS unit cell contrary to the step edge in the lower part of the figure. We also found that a considerable number of adatom sites were imaged as

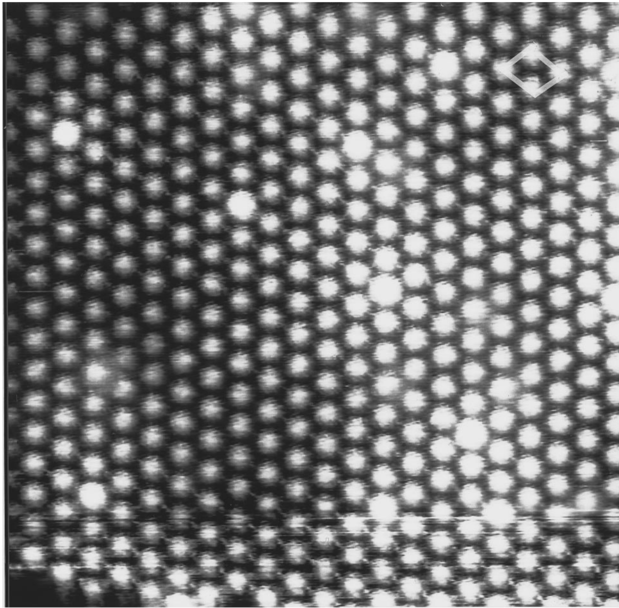

FIG. 2. A 14×14 nm^2 empty state image of the $\sqrt{3}\times\sqrt{3}$ reconstruction which appeared at the edge of the cleaved surface where the implanted B atom accumulated. The sample bias voltage was $+1.4$ V. The tunneling current was 0.3 nA. A unit cell of the $\sqrt{3}\times\sqrt{3}$ reconstruction is indicated at the upper right corner of the figure.

dark protrusions in the 7×7 domain. No such dark protrusion was observed at the 7×7 domain in the middle of the cleaved cross section. Thus, the dark adatom of the 7×7 structure is characteristic of the transient region.

The disordered phase and its boundary with the 7×7 structure were observed by high-resolution STM images as shown in Figs. 4 and 5, which are images of positive and negative bias voltage. The disordered phase is terminated at the boundaries with the region of the 7×7 structure. In the STM image of the positive bias (Fig. 4), we see bright protrusions arranged with $\sqrt{3}\times\sqrt{3}$, 2×2, and $c(2\times4)$ local order. This disordered phase is a stable structure with a certain concentration of B atoms in the surface layer, although a similar disordered structure is reported for a metastable structure of the quenched Si(111) clean surface.[12–15]

We determined sites which give bright/dark protrusion images in Figs. 4 and 5. First, we find that the 7×7 region extended at the upper side of Figs. 4 and 5 terminated at the boundary of the disordered phase by faulted half unit cell (AA' line in Fig. 6) based on the fact that the unfaulted half unit is imaged darker than the faulted half unit in the STM image of the 7×7 reconstruction with the negative sample bias voltage.[26] We also confirm that the boundary terminated

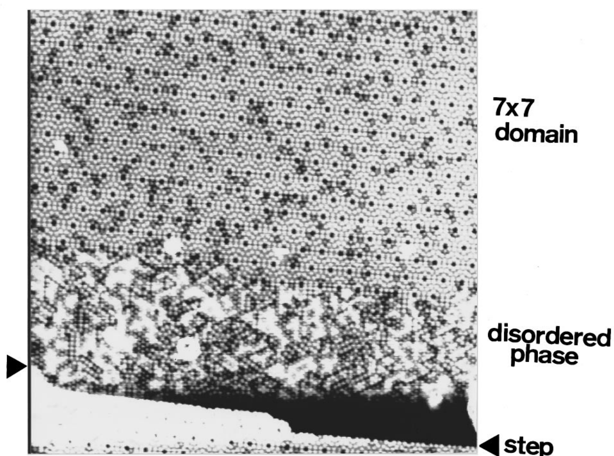

FIG. 3. A 70×70 nm^2 empty state image of the transient region between the $\sqrt{3}\times\sqrt{3}$ and the 7×7 region. It appeared on the region where the implanted B concentration drastically changed from an extremely large to a negligible value. The sample bias voltage was $+2.0$ V. The tunneling current was 0.3 nA.

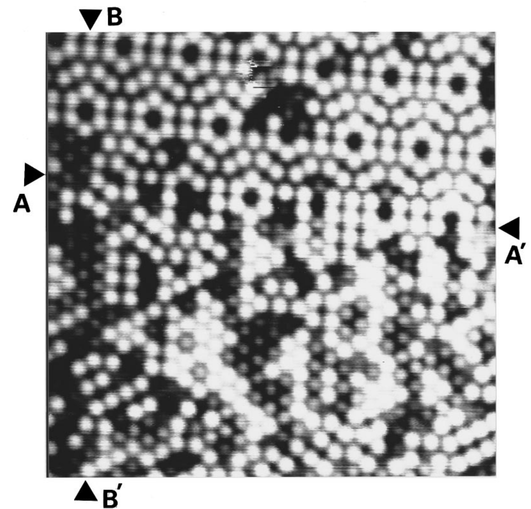

FIG. 4. A 20×20 nm^2 empty state image of the disordered phase in the transient region. The sample bias voltage was $+1.4$ V. The tunneling current was 0.3 nA. The symbols A, A', B, and B' help the reader recognize the correspondence of the position to the negative bias STM image (Fig. 5).

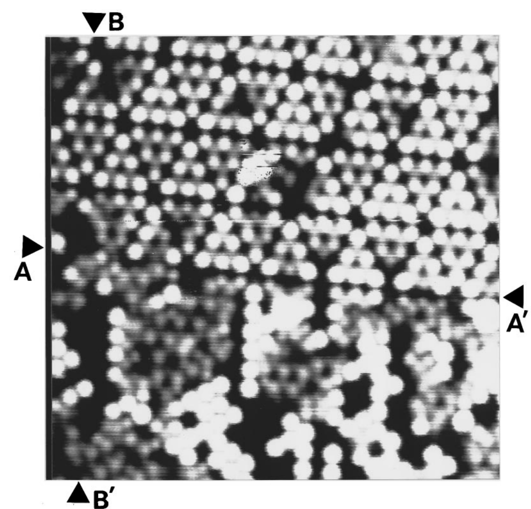

FIG. 5. A 20×20 nm^2 image of the disordered phase in the transient region. The sample bias voltage was -1.3 V. The tunneling current was 0.3 nA. Although this image drifted a little bit to the lower side, most of all the scanned area corresponds to that in Fig. 2. The symbols A, A', B, and B' help the reader recognize the correspondence of the position to the positive bias STM image (Fig. 4).

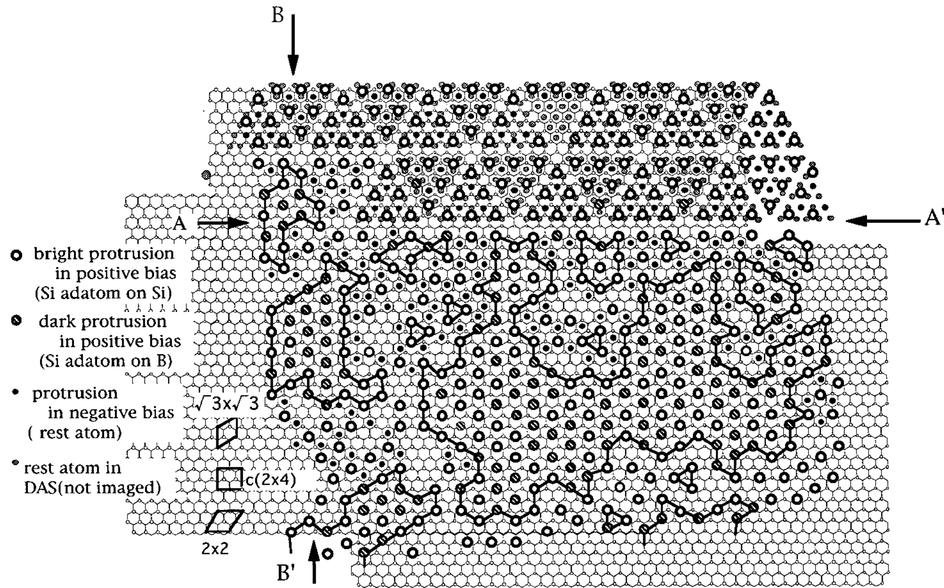

FIG. 6. A map of the disordered phase illustrating protrusions observed in the positive bias (Fig. 4) and the negative bias (Fig. 5) STM. As indicated in the left-hand side of the figure, three symbols represent the bright and dark protrusions in the positive bias STM image and the protrusion in the negative bias STM image. The rest atom in the 7×7 DAS unit is also indicated by a special mark to clarify the boundary of the 7×7 domain. The local domains with the $\sqrt{3}\times\sqrt{3}$ reconstruction are surrounded by the line to help the reader's recognition. Examples of the $\sqrt{3}\times\sqrt{3}$, $c(2\times4)$, and 2×2 unit cell are also shown in the figure. The A, A', B, and B' help the reader recognize the correspondence to Figs. 4 and 5.

by the faulted half unit through the cleavage angle of the surface with respect to the (111) wafer plane. In Fig. 6 of the 1×1 array of hexagons, we marked adatom positions of the 7×7 unit cell by large open circles, and atoms in the stacking-fault layer by shaded small circles. In the 1×1 array, the atoms in the third layer (the layer just below the stacking-fault layer) are indicated by small open circle. Thus, the adatom site of the 7×7 reconstruction ($T4$ site) is on the small open circle. For the atom in the second layer (stacking-fault layer), the stacking-fault site (hollow site) is at the center of the hexagons, and the normal-stacking site is the corner of the hexagons.

Following this definition of the site occupancy, we marked protrusions that appeared at the $T4$ site (i.e., adatom site) in the disordered phase of the positive bias image on the 1×1 mesh. The bright protrusions are at positions marked as large open circles in Fig. 6. Some dark protrusions noticed in the disordered phase and also in the 7×7 regions are marked by hatched large circles. The large open and hatched circles in the disordered region arrange in $\sqrt{3}\times\sqrt{3}$ locally (the $\sqrt{3}\times\sqrt{3}$ local domains are shown in Fig. 6) and in 2×2 and/or $c(2\times4)$. The disordered region is divided into two domains, the $\sqrt{3}\times\sqrt{3}$ local domain and the domain boundary consisting of 2×2 and/or $c(2\times4)$ short-range order.

Table I summarizes the appearance of the bright and dark protrusions at the *adatom site* in the positive and the negative bias images. In the negative bias STM image, protrusions were also observed at some adatom sites ($T4$ site). The correspondence between the positive and the negative protrusions at the adatom site is indicated in the table.

In the negative bias STM image of the 7×7 domain in Fig. 5, we see some intensity from *rest atoms* which are located at the center of adatoms (according to DAS model[3]). We marked their position in Fig. 6 by solid circles; they are located at the hollow site (center of the hexagon) in the faulted half unit cell, while they are at the normal-stacking site (corner of the hexagon) in the unfaulted half unit cell. In the disordered phase, we also recognize traces of protrusions at the site staggered to the to the adatom site outside $\sqrt{3}\times\sqrt{3}$ local domains (i.e., the gap area between $\sqrt{3}\times\sqrt{3}$ local domains). We examined their positions very carefully to find the hollow site as was marked by solid circles in Fig. 6. We cannot see any trace of contrast in the local $\sqrt{3}\times\sqrt{3}$ domain, except for those on the adatom site.

The traces of protrusions found in the gap area between the $\sqrt{3}\times\sqrt{3}$ local domains are similar in contrast to those seen in the 7×7 domain in STM images of the both bias polarities. Since the protrusions at the staggered site to the adatom have been interpreted as due to the rest atom of the DAS model[27] in the 7×7 domain, the traces of the negative bias protrusion at the staggered site might also be rest atoms in the gap area between $\sqrt{3}\times\sqrt{3}$ local domains. Noting that

TABLE I. Image contrast of the protrusion at the adatom site in positive and negative bias STM.

Domain		Positive bias	Negative bias
7×7		bright dark	bright not imaged
Disordered	$\sqrt{3}\times\sqrt{3}$ local domain	bright dark	bright not imaged
	gap area between $\sqrt{3}\times\sqrt{3}$ local domains [2×2 and/or $c(2\times4)$]	bright	not imaged

these rest atoms (solid circles in Fig. 6) have to have back bonds with the atoms at the sites marked by small open circles in Fig. 6, the protrusions at the adatom site are found definitely to be adatoms at $T4$ sites, which have bonds to the atoms at the normal-stacking site (corner of the hexagon). As will be discussed below, we confirmed that almost all the adatoms, up to the phase boundary AA' in Fig. 6, bond with atoms of the normal stacking.

IV. DISCUSSIONS

As described in above section, the disordered phase is correlated to the transient region of the B distribution from a negligible to an extremely large value. In the following, we first discuss the distinction of the B-related and the Si-related protrusions in the STM image. Based on this discussion, we analyze the atomic arrangement of the B and the Si atom in the disordered phase. It is followed by the discussion on the role of the Si atom which disturbs the B-induced $\sqrt{3}\times\sqrt{3}$ reconstruction. The role of the B atom to disturb the 7×7 reconstruction is also discussed as well. Finally, we consider the reason why the disordered phase appeared to get between the 7×7 domain.

In previous STS studies,[6,7] it has been established that the bright and the dark protrusions in the positive bias STM of the B-induced $\sqrt{3}\times\sqrt{3}$ reconstruction are due to the Si adatom at the $T4$ site on the subsurface Si and the subsurface B atom, respectively. This is due to the following reason.[6–8] The dangling bond of the Si adatom at $T4$ site on the Si subsurface is principally half filled.[24,25] This causes the bright protrusion for the Si adatom on the Si subsurface atom in both the positive and the negative bias STM images. However, the $T4$ adatom site on the Si subsurface atom is not favorable for the B atom anymore because of the short bond length of Si-B. The B atom favors the $S5$ subsurface site under the Si adatom to release the bond angle stress. In this case, a charge is transferred from the Si adatom to the B subsurface site. Thus, the Si adatom on the B subsurface site is imaged as a dark protrusion in the positive bias STM (empty state image), and is not imaged in the negative bias STM (occupied state image).

Since the occupation of the B atom at the $S5$ site comes from the *local* stress with the short Si-B bond length, we can safely expect that the B atom takes the $S5$ site under the Si-adatom in the transient region with an insufficient number of B atoms for the $\sqrt{3}\times\sqrt{3}$ structure. In this case, all the adatom site with the B atom at the $S5$ site are imaged as the dark protrusion in the positive bias STM, and are not imaged in the negative bias STM as well as those in the complete $\sqrt{3}\times\sqrt{3}$ domain. Actually, most of all the site, shown by the hatched large circle in Fig. 6, present the above image characteristic, whether the protrusion is in the $\sqrt{3}\times\sqrt{3}$ local domain or not. Thus, we regard all the dark protrusion in the positive bias STM images as the Si adatom on the B atom at $S5$ site.

On the other hand, all the bright protrusion in the positive bias STM (the large open circle) are regarded to be due to the Si adatom on the subsurface Si atom for the following reasons. In the 7×7 domain and the $\sqrt{3}\times\sqrt{3}$ local domain, most of all the site with the bright protrusion in the positive bias STM was also imaged as the bright protrusion in the nega-

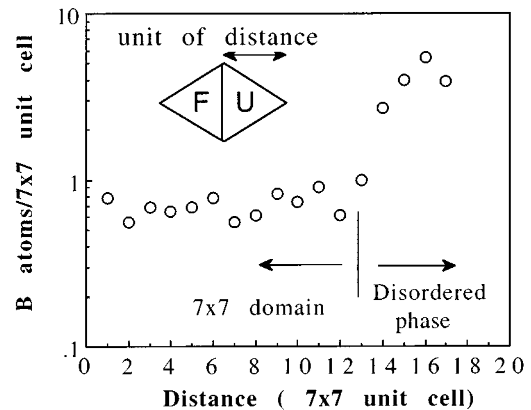

FIG. 7. The distribution of subsurface B atoms along the direction perpendicular to the boundary between the 7×7 domain and the disordered phase. The surface density of the B atom was counted as the number of the B atom included in the 7×7 unit cell. The unit of the distance along the line perpendicular to the 7×7-disordered phase boundary is illustrated in the figure.

tive bias STM. This agrees with the characteristic half-filled dangling bond state of the Si adatom on the subsurface Si atom in the 7×7 DAS unit cell[24–26] and the B-induced $\sqrt{3}\times\sqrt{3}$ domain.[6,7] At the gap area between $\sqrt{3}\times\sqrt{3}$ local domains, the bright protrusions are arranged with the local order of the $c(2\times4)$ or the 2×2. The protrusion in the positive bias STM appeared at the staggered site to the protrusion in the negative bias STM. This is attributed to the Si adatom arrangement with the local order of $c(2\times4)$ or 2×2 over the Si rest atom layer. The 2×2 unit cell with the combination of the Si adatom and the Si rest atom includes two dangling bonds; one on the rest atom and one on the adatom. The $c(2\times4)$ unit cell also includes four dangling bonds, two on the rest atoms and two on the adatoms. On these staggered configurations of the Si adatom and the Si rest atom, the charge is transfered from the Si adatom to the Si rest atom.[28,29] This results in the filled rest atom band and the empty adatom band. Thus, the Si adatom and the Si rest atom are expected to be observed as the protrusion in the positive and the negative bias STM, respectively. In fact, Fig. 6 indicates that the bright protrusion in the positive bias STM (empty state image) appeared at $T4$ site, which is occupied by the adatom, while the protrusion in the negative bias STM (occupied state image) appeared at the hollow site on the underlying network, which is occupied by the rest atom. Therefore, we attribute the bright protrusion of the gap area in the positive bias STM to the Si adatom over the Si atom arranged in the rest atom layer.

Based on the above discussion, we distinguished the B-related protrusion from the B-free protrusion in our STM images. At a glance, it is clear that a small number of the B atoms (the dark protrusion in the positive bias STM; i.e., the hatched large circle) is included in the 7×7 domain neighboring to the disordered phase. Behind the boundary, the number of B atoms drastically increases and the surface structure changes from the 7×7 to the disordered phase. By counting the number of the bright and the dark protrusions at the transient region, we estimate the distribution of B atoms on the cleaved surface numerically. The distribution around the disordered phase is shown in Fig. 7. Here, the surface density of the B-related protrusion was counted as a function

of the distance along the direction normal to the boundary between the disordered phase and the adjacent 7×7 domain. We set a network of the 7×7 unit cell, and count the number of B-related protrusions in the 7×7 unit mesh. The average density along the column parallel to the boundary is presented. The result indicates that approximately one B atom is included in the 7×7 unit cell at the adjacent 7×7 domain. However, the B concentration jumps at the boundary and reaches to ~7 atoms per 7×7 unit cell in the disordered phase. Just after the jump of the local B concentration, the $\sqrt{3}\times\sqrt{3}$ domain starts to nucleate locally in the disordered region. This means that the 7×7 reconstruction bears up against the B inclusion up to approximately one atom per unit cell. But, the 7×7 reconstruction is destroyed by the B inclusion above several atoms per unit cell. This results in the disordered phase with the $\sqrt{3}\times\sqrt{3}$, $c(2\times4)$, and 2×2 local atomic arrangements. Shen *et al.* has studied the metastable area of the quenched Si(111) surface of the B-doped ($\sim10^{19}$ cm^{-3}) wafer and has reported that the 7×7 DAS structure lasts against the B inclusion up to two atoms per unit cell.[9] This is consistent with our result on the cleaved surface of the B-implanted Si wafer.

The inclusion of a considerable number of B atoms causes the disordered phase with the mixture of the $\sqrt{3}\times\sqrt{3}$, $c(2\times4)$, and 2×2 local atomic arrangement. Judging from the spatial distribution of the bright and the dark protrusion in the positive bias STM, the following are found to be the characteristics of the disordered phase. The B atom is included only in the $\sqrt{3}\times\sqrt{3}$ local domain. The gap area of the $c(2\times4)$ or 2×2 local orders never includes the B atom. Among $\sqrt{3}\times\sqrt{3}$ domains of the disordered phase, the B atom tends to concentrate on sizable $\sqrt{3}\times\sqrt{3}$ domains. We think that these characteristics of the disordered phase are due to the energetics of the local atomic arrangements with and without B subsurface atoms. A theoretical calculation has showed that the Si adatom–B subsurface-atom configuration is favored over the B adatom–Si subsurface site configuration by 0.31 eV (1×1 cell).[6] Moreover, the $\sqrt{3}\times\sqrt{3}$ reconstruction is the most favorable arrangement of the adatom with respect to the general rule of the surface reconstruction; the reduction of the number of the surface dangling bond. Thus, the B-rich surface principally favors to extend the $\sqrt{3}\times\sqrt{3}$ local domain with the subsurface B atom, as is usually observed on the Si(111) surface with the B atoms of the saturation coverage.[4–7] This causes the $\sqrt{3}\times\sqrt{3}$ local domain with B subsurface atom in the disordered phase. However, the B concentration at the transient region is not enough to cover all the surface with the B-induced $\sqrt{3}\times\sqrt{3}$ reconstruction. Therefore, the B-deficient area is necessarily left in the gap between $\sqrt{3}\times\sqrt{3}$ local domains. Usually, the Si(111) surface without B atoms takes the energetically most favorable 7×7 reconstruction. But, the gap area was not large enough to accommodate the unit cell of the 7×7 reconstruction. In this case, the gap area is expected to take the other reconstruction of a low surface energy. To reduce the number of the surface dangling bond, the $\sqrt{3}\times\sqrt{3}$ adatom arrangement is the most favorable even for the B-deficient gap area. However, a theoretical calculation has showed that the 2×2 arrangement is energetically preferable over the $\sqrt{3}\times\sqrt{3}$ arrangement in the Si adatom–Si rest atom configuration without the subsurface B atom.[29] This comes from the balance between the reduction of the surface dangling bond and the relaxation of the stress accompanied with the adatom configuration. The dangling-bond density of the 2×2 arrangement is the second smallest; it is still larger than that of the $\sqrt{3}\times\sqrt{3}$ arrangement. But, the longer distance between the adatom of the 2×2 arrangement is more effective to release the adatom-induced stress. This makes the total energy of the 2×2 arrangement lower than that of the $\sqrt{3}\times\sqrt{3}$ arrangement. The $c(2\times4)$ arrangement has been also reported to have the low surface energy nearly the same as that of the 2×2 arrangement.[30] Hence, it is reasonable that the energetically preferable $c(2\times4)$ and the 2×2 local atomic arrangements appear in the B-deficient gap area.

As discussed above, the coexistence of the $\sqrt{3}\times\sqrt{3}$, $c(2\times4)$, and 2×2 local arrangement in the disordered phase is basically explained by the energetics of the local atomic arrangement with and without the B subsurface atom. Here, B atoms take the subsurface site and gather locally to extend the energetically favorable $\sqrt{3}\times\sqrt{3}$ domain. However, we found that the $\sqrt{3}\times\sqrt{3}$ local domain still contains a considerable number of Si atoms in the subsurface layer, which are observed as bright protrusions in the $\sqrt{3}\times\sqrt{3}$ local domain. These subsurface Si atoms are regarded as the disturbance of the B-induced $\sqrt{3}\times\sqrt{3}$ reconstruction. The STM images of the disordered phase (Figs. 4 and 5) show that the site on the subsurface Si atom tends to extend as one-dimensional chains inside the $\sqrt{3}\times\sqrt{3}$ local domain. This means that the B-induced $\sqrt{3}\times\sqrt{3}$ reconstruction persists against the one-dimensional chainlike aggregation of the subsurface Si atoms. However, the lack of the two-dimensional aggregation of Si subsurface atoms into a considerable size suggests that the B-induced $\sqrt{3}\times\sqrt{3}$ reconstruction does not persist against the two-dimensional aggregation of the subsurface Si atoms. We think that the intolerance of the B-induced $\sqrt{3}\times\sqrt{3}$ reconstruction against the two-dimensional aggregation of the subsurface Si atom is due to the following reason. The equitriangular arrangement with the side distance of $\sqrt{3}a$ [a is the length of side of the 1×1 unit cell on the ideal Si(111) surface] is necessary for the subsurface Si atom to extend the two-dimensional aggregation. But, as described in the above paragraph, the Si adatom–Si subsurface-atom configuration does not favor the $\sqrt{3}\times\sqrt{3}$ arrangement. Therefore, the B-induced $\sqrt{3}\times\sqrt{3}$ local domain can include the one-dimensional alignment of the subsurface Si atom, but does not persist for the two-dimensional aggregation of the subsurface Si atom.

On the contrary to the subsurface Si atom in the B-induced $\sqrt{3}\times\sqrt{3}$ local domain, the subsurface B atom in the 7×7 domain is regarded as the disturbance to the 7×7 DAS reconstruction. In this respect, the boundary between the disordered phase and the neighboring 7×7 domain is interesting because it is expected to represent the critical phenomena of the destruction of the the 7×7 reconstruction by the B atom. As illustrated in Fig. 6, the 7×7 DAS region was always terminated by the faulted halves of the DAS unit cell on the terrace. Moreover, we found that the closest adatom of the disordered phase to the boundary takes the counterpart site to the corner adatom of the 7×7 reconstruction. We think that these characteristics of the boundary come from the stability of the faulted half of the 7×7 DAS unit cell and the necessity of the dimer chain to construct the

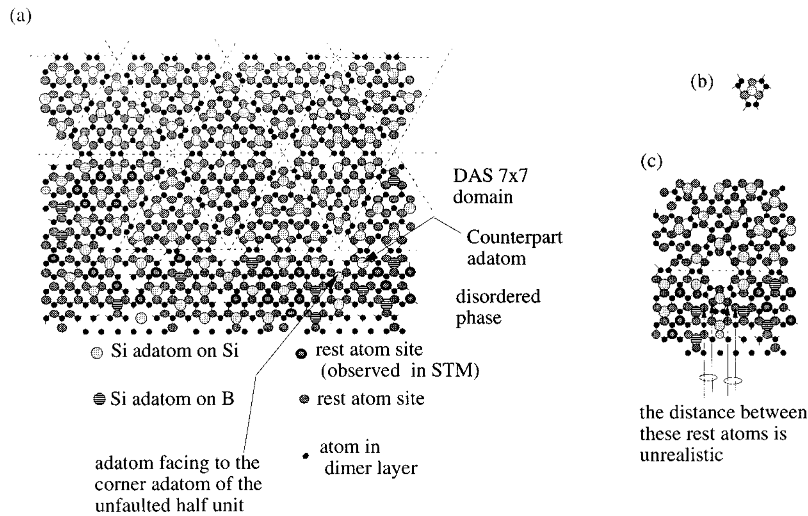

FIG. 8. Models of the Si atom arrangement in the rest atom layer at the disordered phase. Based on the observed site of the adatom and the rest atom (around the cross point of AA' and BB' line in Fig. 6), the site of invisible atom in the rest atom layer is inferred. Adatoms, rest atoms, and atoms in the dimer layer are illustrated by symbols as indicated in the figure. (a) The rest atom layer has no stacking fault in the disordered phase. This is consistent with the observed adatom and the rest atom site in the disordered phase. (b) The smallest unit of adatom-rest atom-dimer combination. This works as the trigger to construct the stacking fault in the 7×7 reconstruction when the adatom takes the site facing to the corner adatom of the unfaulted half unit. (c) The stacking fault is introduced into the disordered phase by the adatom facing to the corner adatom of the unfaulted half unit in the 7×7 domain. However, this results in the frustrated arrangement of the atom in the rest atom layer as indicated in the figure.

faulted area. The stability of the faulted half unit has been pointed out by Hoshino *et al.*[31] They have found the leading role of the faulted halves in the 7×7 DAS structure formation during the $1\times1\rightarrow7\times7$ transition. From their finding, they have proposed that the faulted half is the energetically favorable smallest unit cell of the Si(111) surface. On the other hand, the faulted half unit is always surrounded by the dimer chain [Fig. 8(a)]. This dimer chain is necessary to construct the faulted area on the Si(111) surface. Then, to construct the dimer at the boundary, the edge adatom in the faulted half unit needs the counter part adatom in the disordered phase as illustrated in Fig. 8(a). Actually, a theoretical study has indicated that the dimer-adatom pair along the outside edge is responsible for stabilizing the faulted half unit.[32] Thus, it is reasonable that the 7×7 domain is terminated by the faulted halves with the counterpart adatom in the disordered phase to the edge adatoms of the faulted half unit.

Furthermore, we found that the adatom in the disordered phase arranges to conserve the corner hole in corporation with the corner adatom in the 7×7 domain (Fig. 4), though the memory of these neighboring 7×7 domain did not continue further to the inside arrangement of adatoms of the disordered phase. To construct the corner hole at the boundary, one more adatom, which faces to the corner adatom of the unfaulted adatom, is necessary in addition to the counterpart adatom [Fig. 8(a)]. Here, the problem is whether the stacking fault is introduced into the disordered layer by the adatom arrangement to conserve the corner hole or not. In the 7×7 reconstruction, the counterpart adatom connects to the atomic arrangement of the unfaulted half unit. However, the adatom facing to the corner adatom of the unfaulted adatom introduces the stacking fault. In the analogy of this 7×7 reconstruction, we expect that the stacking fault is introduced into the disordered phase by the adatom facing to the corner adatom of the unfaulted half unit. We examine this possibility by analyzing the arrangement of the rest atom in the disordered phase. In the negative bias STM, the rest atom, which does not bond to the adatom, was imaged as a protrusion.[26,27] The site of the invisible rest atom, which bonds to the adatom, is inferred from the adatom site observed in STM. We utilized the observed adatom and rest atom sites as the clue to construct the atomic arrangement of the rest atom layer in the disordered phase. The atomic arrangement of the rest atom layer is constructed to be consistent with the observed adatom and rest atom sites in the disordered phase. The result is illustrated in Fig. 8(a). On the contrary to our expectation, all of the observed atomic arrangement is consistently reproduced with the assumption that the adatom facing the corner adatom of the unfaulted half unit does not introduce the stacking fault. If we assume that the stacking fault is introduced into the disordered phase by the atomic arrangement of Fig. 8(b) with the adatom facing to the corner adatom of the unfaulted half unit, we obtained the nonrealistic arrangement of the rest atom as indicated in Fig. 8(c). Thus, we conclude that the stacking fault is not introduced into the B-related disordered phase even though the corner hole is constructed at the boundary. The B atom prevents the extension of the faulted half unit, and results in the destruction of the 7×7 domain.

Finally, we briefly discuss the reason why the disordered phase appeared as getting between the 7×7 domain in the transient region. Our results indicate that the B-related disordered phase preferentially nucleates at the the step on the lower terrace. A similar preference of the nucleation has been reported for a Au-induced 5×2 reconstruction on the Si(111) surface.[33,34] The preference of the nucleation of the 7×7 reconstruction at the edge of the outer step has also been reported in the phase transition between the 7×7 and

the 1×1 phase on the Si(111) surface.[35] The step-related strain has been pointed out as the origin of the preference.[36] However, besides the strain, the mass transfer and the related growth of the step, which happen in the heat process, should be considered in our case. In studies of the homoepitaxial growth on the Si(111) surface, two kinds of the step edge have been observed; a straight step terminated by the unfaulted half unit and a zig-zag step terminated by the faulted half unit.[37–39] The straight edge with the unfaulted half unit means that the addition of the faulted half to the unfaulted step edge is energetically unfavorable. In our result, all the step edge in the transient region was straight and was terminated by the unfaulted half unit. This suggests that the step growth plays a role in the formation of the landscape of the transient region. However, at the present stage, we have no evidence which is the dominant factor for the preference.

V. SUMMARY

We observed the {111} cleaved cross-sectional surface of the heavily B-implanted Si(111) wafer. As cleaved, the cross section included many defects at the edge region where the drastic change of implanted B atom is expected. This made the atomically resolved STM observation of the cross section of the interesting region difficult. However, the subsequent annealing extended a flat region at the edge and enabled us an atomically resolved STM observation. On this cross section, the $\sqrt{3}\times\sqrt{3}$ reconstruction was observed on the region where the implanted B atom accumulated, whereas the 7×7 reconstruction appeared in the region that the implanted B atom did not reach. Between the $\sqrt{3}\times\sqrt{3}$ and the 7×7 reconstruction, the transient region with the disordered phase was observed. The disordered phase extended on the lower terrace from the step edge. On the terrace, the disordered phase connected to the 7×7 domain terminated by the faulted halves of the 7×7 DAS unit cell.

Based on the brightness of the protrusion observed in the positive bias STM, the site with the Si adatom on the subsurface B atom was distinguished from that on the subsurface Si atom. The contrast of the brightness is caused by the characteristic subsurface site of the B atom under the Si adatom. By counting the number of the B-induced protrusions, we found that the 7×7 reconstruction lasts against the inclusion of approximately one atom per 7×7 unit cell, whereas the 7×7 reconstruction is changed into the disordered phase by the inclusion of several B atoms per 7×7 unit cell. The disordered phase was the mixture of the $\sqrt{3}\times\sqrt{3}$, the $c(2\times4)$ and the 2×2 local reconstructions. In the disordered phase, the B atom gathered and formed the local domain of the $\sqrt{3}\times\sqrt{3}$ reconstruction. As a result, the B deficient region was left between $\sqrt{3}\times\sqrt{3}$ local domains. The B deficient region showed the $c(2\times4)$ and 2×2 local reconstructions. The $\sqrt{3}\times\sqrt{3}$ and $c(2\times4)$ or (2×2) are energetically stable structures of the B-rich and B-free Si(111) surfaces, respectively. Thus, we think that the observed disordered phase is basically the result of the energetics to minimize the total energy of the surface where the B coverage is less than the saturation value to construct the perfect $\sqrt{3}\times\sqrt{3}$ reconstruction.

In the transient region, we also found that the B-induced $\sqrt{3}\times\sqrt{3}$ local domain lasts against the inclusion of the one dimensionally aggregated Si adatoms on the subsurface Si atom. However, it does not persist for the two-dimensional aggregation of the subsurface Si atom into a considerable size. We consider that it is due to the instability of the $\sqrt{3}\times\sqrt{3}$ arrangement of the Si adatom-Si subsurface-atom configuration. Moreover, at the boundary between the disordered phase and the 7×7 domain, the closest adatom in the disordered phase to the 7×7 domain was observed to take the counterpart site to the edge adatom in the adjacent faulted half unit of the 7×7 domain. The corner hole was also conserved at the boundary. The counterpart adatom is necessarily introduced to construct the dimer chain at the boundary, which is responsible for the stability of the faulted half unit. However, based on the arrangement of the observed adatom and rest atom sites, we found that the stacking fault is not introduced into the disordered phase through the corner hole at the boundary.

ACKNOWLEDGMENTS

The authors would like to thank M. Kawata of NEC Corporation for preparing the B-implanted Si(111) sample. This work was financially supported by a Grant-in-Aid (No. 08230212) for Scientific Research from the Ministry of Education, Science and Culture of Japan.

*Present address: Toshiba Corporation, Kawasaki 210, Japan.
†Present address: Sharp Corporation, Osaka 545, Japan.

[1] E. Landi, A. Armigliato, S. Solmi, R. Kogler, and E. Wieser, Appl. Phys. A **47**, 359 (1988).
[2] S. Solmi, E. Landi, and F. Baruffaldi, J. Appl. Phys. **68**, 3250 (1990).
[3] K. Takayanagi, Y. Tanishiro, S. Takahashi, and M. Takahashi, Surf. Sci. **164**, 367 (1985).
[4] V. V. Korobtsov, V. G. Lifshits, and A. V. Zotov, Surf. Sci. **195**, 466 (1988).
[5] H. Hirayama, T. Tatsumi, and N. Aizaki, Surf. Sci. **193**, L47 (1988).
[6] I.-W. Lyo, E. Kaxiras, and Ph. Avouris, Phys. Rev. Lett. **63**, 1261 (1989).
[7] P. Bedrossian, R. Meade, K. Mortensen, D. M. Chen, J. A. Golovchenko, and D. Vanderbilt, Phys. Rev. Lett. **63**, 1257 (1989).
[8] E. Kaxiras, K. C. Pandey, F. J. Himpsel, and R. M. Tromp, Phys. Rev. B **41**, 1262 (1990).
[9] T.-C. Shen, C. Wang, J. W. Lyding, and J. R. Tucker, Phys. Rev. B **50**, 7453 (1994).
[10] T. M. H. Wong, A. W. Mckinnon, and M. E. Welland, Surf. Sci. **328**, 227 (1995).
[11] A. V. Zotov, M. A. Kulakov, S. V. Ryzhkov, A. A. Saranin, V. G. Lifshits, B. Bullermer, and I. Eisele, Surf. Sci. **345**, 313 (1996).
[12] R. S. Becker, J. A. Golovchenko, G. S. Higashi, and B. S. Swartzentruber, Phys. Rev. Lett. **57**, 1020 (1986).
[13] M. Tomitori, F. Iwawaki, N. Hirano, F. Katsuki, and O. Nishikawa, J. Vac. Sci. Technol. A **8**, 222 (1990).
[14] Y.-N. Yang and E. D. Williams, Phys. Rev. Lett. **72**, 1862 (1994).
[15] K. Kumamoto, T. Hoshino, K. Kokubun, T. Ishimaru, and I. Ohdomari, Phys. Rev. B **52**, 10 784 (1995).
[16] M. Y. Tsai and B. G. Streetman, J. Appl. Phys. **50**, 183 (1979).

[17] W. Gopel and G. Neuenfelt, Surf. Sci. **55**, 362 (1976).
[18] R. M. Feenstra, W. A. Thompson, and A. P. Fein, Phys. Lett. **56A**, 608 (1986).
[19] J. A. Stroscio, R. M. Feenstra, and A. P. Fein, J. Vac. Sci. Technol. A **5**, 838 (1987).
[20] R.M. Feenstra, J. A. Stroscio, and A. P. Fein, Surf. Sci. **181**, 295 (1987).
[21] R. M. Feenstra and J. A. Stroscio, Phys. Rev. Lett. **59**, 2173 (1987).
[22] R. M. Feenstra and M. A. Lutz, Surf. Sci. **243**, 151 (1991).
[23] L. Csepregi, J. W. Mayer, and T. W. Sigmon, Appl. Phys. Lett. **29**, 92 (1976).
[24] R. J. Hamers, R. M. Tromp, and J. E. Demuth, Phys. Rev. Lett. **56**, 1972 (1986).
[25] J. Northrup, Phys. Rev. Lett. **57**, 154 (1986).
[26] R. J. Hamers, Annu. Rev. Phys. Chem. **40**, 531 (1989).
[27] R. Wolkow and Ph. Avouris, Phys. Rev. Lett. **60**, 1049 (1988).
[28] R. S. Becker, B. S. Swartzentruber, J. S. Vickers, and T. Klitsner, Phys. Rev. B **39**, 1633 (1989).
[29] R. Meade and D. Vanderbilt, Phys. Rev. B **40**, 3905 (1989).
[30] J. Kanamori, Solid State Commun. **50**, 363 (1984).
[31] T. Hoshino, K. Kuramoto, K. Kokubun, T. Ishimaru, and I. Ohdomari, Phys. Rev. B **51**, 14 594 (1995).
[32] M. C. Payne, J. Phys. C **20**, L983 (1987).
[33] Y. Tanishiro and K. Takayanagi, Ultramicroscopy **31**, 20 (1989).
[34] W. Swiech, E. Bauer, and M. Mundshau, Surf. Sci. **253**, 283 (1991).
[35] N. Osakabe, Y. Tanishiro, K. Yagi, and G. Honjo, Surf. Sci. **102**, 424 (1981).
[36] D. Haneman, Phys. Rev. B **25**, 1370 (1982).
[37] R. J. Hamers, U. K. Kohler, and J. E. Demuth, Ultramicroscopy **31**, 10 (1989).
[38] H. Tochihara, W. Shimada, M. Itoh, H. Tanaka, M. Udagawa, and I. Sumita, Phys. Rev. B **45**, 11 332 (1992).
[39] T. Hasegawa, M. Kohno, S. Hosaka, and S. Hosoki, Phys. Rev. B **48**, 1943 (1993).